Archive of Applied Mechanics (2024) 94:81–98
https://doi.org/10.1007/s00419-023-02509-x

ORIGINAL

Plastiras Demetriou · Gianluca Rizzi · Angela Madeo

Reduced relaxed micromorphic modeling of harmonically loaded metamaterial plates: investigating boundary effects in finite-size structures

Received: 16 May 2023 / Accepted: 4 October 2023 / Published online: 29 November 2023

Abstract In this paper, we propose an approach for describing wave propagation in finite-size microstructured metamaterials using a reduced relaxed micromorphic model. This method introduces an additional kinematic field with respect to the classical Cauchy continua, allowing to capture the effects of the underlying microstructure with a homogeneous model. We show that the reduced relaxed micromorphic model is not only effective for studying infinite-size metamaterials, but also efficient for numerical simulations and analysis on specimens of finite size. This makes it an essential tool for designing and optimizing metamaterials structures with specific wave propagation properties. The proposed model's efficiency is assessed through numerical simulations for finite-size benchmark problems, and shows a good agreement for a wide range of frequencies. The possibility of producing the same macroscopic metamaterial with different but equivalent unit cell "cuts" is also analyzed, showing that, even close to the boundary, the reduced relaxed micromorphic model is capable of giving accurate responses for the considered loading and boundary conditions.

Keywords Finite-size metamaterials · Wave propagation · Homogenization · Reduced relaxed micromorphic model

1 Introduction

In recent years, acoustic metamaterials have gathered significant attention for their ability to manipulate mechanical waves in ways that surpass the capabilities of classical materials. These materials are engineered with ad hoc microstructures that can effectively control the propagation of mechanical waves, resulting in unique properties such as negative Poisson's ratio [23,43,55], chiral effects [16,27,28,58,65,66], band gaps [5,10,18,25,30,33,36,40,41,46,87,95], cloaking [14,52,53,62,73], focusing [21,34], channeling [11,39,42,51,83,88], negative refraction [11,47,54,79,93,95], and others [17,26,32,44,56,57,84,94]. The potential applications of acoustic metamaterials are broad, including also noise reduction, imaging, and communication. While progress has been made in designing, fabricating, and modeling such materials, several challenges remain. One of the main obstacles is to achieve the ability of modeling the desired acoustic properties across a wide frequency range and at a large scale, which is crucial for real-world engineering applications. In recent papers [1,24,64,67–70,86] we have shown that the reduced relaxed micromorphic model performs well in describing the response of infinite-size metamaterials and also for some simple finite-size problems. The importance

P. Demetriou · G. Rizzi (✉)
Faculty of Architecture and Civil Engineering, TU Dortmund, August-Schmidt-Str. 8, 44227 Dortmund, Germany
gianluca.rizzi@tu-dortmund.de

A. Madeo
Head of Chair of Structural Mechanics, Faculty of Architecture and Civil Engineering, TU Dortmund, August-Schmidt-Str. 8, Dortmund, Germany

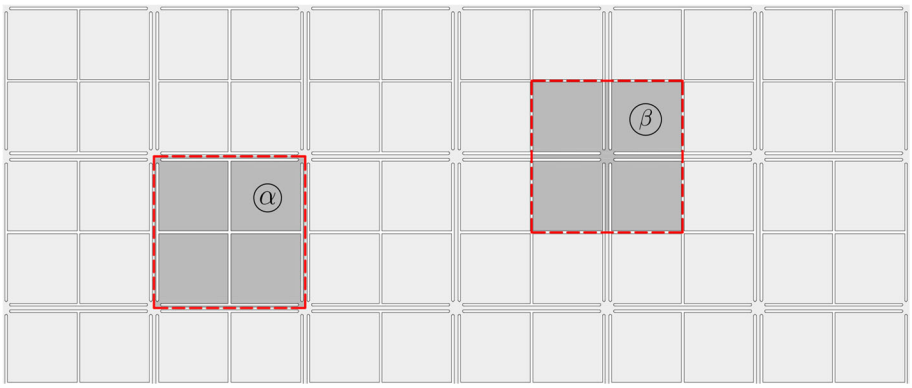

Fig. 1 Two of the possible unit cell "cuts" that can be chosen and whose periodic tailing builds the same infinite metamaterial

of micromorphic models for modeling metamaterials and heterogeneous media has also been acknowledged through the development of homogenization techniques in quasi-static regime [2–4,6,9,12,15,29,35,45,49,50,63,71,72,74,76,77,82,85,89] as well as, more recently, in the dynamic regime [7,8,13,19,20,37,38,75,78,80,81,90–92]. However, in order to model dispersion at frequencies higher than the acoustic modes and band gap, enriched models of the micromorphic type must be used at the homogenized scale. To our knowledge, the problem proposed in the present paper is the first one which tries to address the fundamental question of homogenized boundary conditions which are representative of complex situations like considering two unit cell "cuts" for different metamaterials. We present this paper as a necessary step to gain the needed insight to proceed toward more complex situations (for example, the effect of the cell's "cut" when the metamaterial is in contact with another homogeneous solid). In the present paper, we show for the first time that the reduced relaxed micromorphic model is well adapted to describe the overall behavior of a metamaterials stemming from different unit cell "cuts," when considering "free" boundaries and "thin" Cauchy bars. The question of studying boundary conditions to be imposed at interfaces between a reduced relaxed micromorphic continuum and another material (e.g., a "thick" Cauchy bar) to reproduce the response of different "α" and "β" cuts is very delicate and will be addressed in forthcoming papers. The present paper wants to establish that the effect of different cell's cuts does not consistently affect the reduced relaxed micromorphic model's performance as far as simple boundary and loading conditions are considered.

Another issue concerns the choice of the unit cell, the fundamental building block of periodic metamaterials, when dealing with finite-size samples. The choice of the unit cell "cut" (see Fig. 1) may induce a different response on the metamaterial's boundary that can propagate inside the bulk material. We show that, for the targeted metamaterial and the chosen applied load, these boundary effects are limited to a region very close to the boundary in almost all cases. This implies that in this case, possible deviation of the reduced relaxed micromorphic model response may be restricted only to small regions very close to the boundary. By understanding the properties of metamaterials' unit cells, their associated boundary effects, and by modeling them through the reduced relaxed micromorphic model, we can better understand how to model the propagation of sound waves in finite-size metamaterials' samples for wide ranges of frequencies and different unit cells. This will allow upscaling and will thus have important implications for fields such as materials science, acoustics, and engineering.

2 The relaxed micromorphic model: a reduced version for dynamics

We introduce here the equilibrium equations, the associated boundary conditions, and the constitutive relations for a reduced version [24,64,67–70] of the relaxed micromorphic model [1,31,48,59–61,86] for dynamic applications.[1] The equilibrium equations and the boundary conditions are derived with a variational approach

[1] The adjective "relaxed" was introduced by some of the authors for the specific micromorphic-type continuum model they pioneered some years ago. The term "relaxed" is related to: (*i*) the fact that the curvature term in the strain energy term of the full model is related to the Curl of the micro-distortion P instead than of its entire gradient and (*ii*) contrarily to classical Mindlin-type models, there are no mixed terms of the type $\langle \nabla u - P, \operatorname{sym} P \rangle$.

thanks to the associated Lagrangian

$$\mathcal{L}(\dot{u}, \nabla\dot{u}, \dot{P}, \nabla u, P) := K(\dot{u}, \nabla\dot{u}, \dot{P}) - W(\nabla u, P)\,, \tag{1}$$

where K and W are the kinetic and strain energy, respectively, defined as[2]

$$\begin{aligned} K(\dot{u}, \nabla\dot{u}, \dot{P}) :=& \frac{1}{2}\rho\,\langle \dot{u}, \dot{u}\rangle + \frac{1}{2}\langle \mathbb{J}_{\mathrm{m}}\,\mathrm{sym}\,\dot{P}, \mathrm{sym}\,\dot{P}\rangle + \frac{1}{2}\langle \mathbb{J}_{\mathrm{c}}\,\mathrm{skew}\,\dot{P}, \mathrm{skew}\,\dot{P}\rangle \\ &+ \frac{1}{2}\langle \mathbb{T}_{\mathrm{e}}\,\mathrm{sym}\nabla\dot{u}, \mathrm{sym}\nabla\dot{u}\rangle + \frac{1}{2}\langle \mathbb{T}_{\mathrm{c}}\,\mathrm{skew}\nabla\dot{u}, \mathrm{skew}\nabla\dot{u}\rangle\,, \end{aligned} \tag{2}$$

$$\begin{aligned} W(\nabla u, P) :=& \frac{1}{2}\langle \mathbb{C}_{\mathrm{e}}\,\mathrm{sym}\,(\nabla u - P)\,, \mathrm{sym}\,(\nabla u - P)\rangle + \frac{1}{2}\langle \mathbb{C}_{\mathrm{c}}\,\mathrm{skew}\,(\nabla u - P)\,, \mathrm{skew}\,(\nabla u - P)\rangle \\ &+ \frac{1}{2}\langle \mathbb{C}_{\mathrm{micro}}\,\mathrm{sym}\,P, \mathrm{sym}\,P\rangle\,, \end{aligned} \tag{3}$$

where $\langle\cdot,\cdot\rangle$ denote the scalar product, the dot represents a derivative with respect to time, $u \in \mathbb{R}^3$ is the macroscopic displacement field, $P \in \mathbb{R}^{3\times3}$ is the non-symmetric micro-distortion tensor, ρ is the macroscopic apparent density, $\mathbb{J}_{\mathrm{m}}$, $\mathbb{J}_{\mathrm{c}}$, $\mathbb{T}_{\mathrm{e}}$, $\mathbb{T}_{\mathrm{c}}$, are 4th-order micro-inertia tensors, and $\mathbb{C}_{\mathrm{e}}$, $\mathbb{C}_{\mathrm{m}}$, $\mathbb{C}_{\mathrm{c}}$ are 4th-order elasticity tensors (see [68,86] for more details). In particular, we report here the structure of the micro-inertia and the elasticity tensors for the tetragonal class of symmetry and in Voigt notation

$$\begin{aligned} &\mathbb{C}_{\mathrm{e}} = \begin{pmatrix} \kappa_{\mathrm{e}}+\mu_{\mathrm{e}} & \kappa_{\mathrm{e}}-\mu_{\mathrm{e}} & \star & \dots & 0 \\ \kappa_{\mathrm{e}}-\mu_{\mathrm{e}} & \kappa_{\mathrm{e}}+\mu_{\mathrm{e}} & \star & \dots & 0 \\ \star & \star & \star & \dots & 0 \\ \vdots & \vdots & \vdots & \ddots & \\ 0 & 0 & 0 & & \mu_{\mathrm{e}}^* \end{pmatrix}, \quad \mathbb{C}_{\mathrm{micro}} = \begin{pmatrix} \kappa_{\mathrm{m}}+\mu_{\mathrm{m}} & \kappa_{\mathrm{m}}-\mu_{\mathrm{m}} & \star & \dots & 0 \\ \kappa_{\mathrm{m}}-\mu_{\mathrm{m}} & \kappa_{\mathrm{m}}+\mu_{\mathrm{m}} & \star & \dots & 0 \\ \star & \star & \star & \dots & 0 \\ \vdots & \vdots & \vdots & \ddots & \\ 0 & 0 & 0 & & \mu_{\mathrm{m}}^* \end{pmatrix}, \\ &\mathbb{J}_{\mathrm{m}} = \rho L_{\mathrm{c}}^2 \begin{pmatrix} \kappa_\gamma+\gamma_1 & \kappa_\gamma-\gamma_1 & \star & \dots & 0 \\ \kappa_\gamma-\gamma_1 & \kappa_\gamma+\gamma_1 & \star & \dots & 0 \\ \star & \star & \star & \dots & 0 \\ \vdots & \vdots & \vdots & \ddots & \\ 0 & 0 & 0 & & \gamma_1^* \end{pmatrix}, \quad \mathbb{T}_{\mathrm{e}} = \rho L_{\mathrm{c}}^2 \begin{pmatrix} \bar{\kappa}_\gamma+\bar{\gamma}_1 & \bar{\kappa}_\gamma-\bar{\gamma}_1 & \star & \dots & 0 \\ \bar{\kappa}_\gamma-\bar{\gamma}_1 & \bar{\kappa}_\gamma+\bar{\gamma}_1 & \star & \dots & 0 \\ \star & \star & \star & \dots & 0 \\ \vdots & \vdots & \vdots & \ddots & \\ 0 & 0 & 0 & & \bar{\gamma}_1^* \end{pmatrix}, \\ &\mathbb{J}_{\mathrm{c}} = \rho L_{\mathrm{c}}^2 \begin{pmatrix} \star & 0 & 0 \\ 0 & \star & 0 \\ 0 & 0 & 4\gamma_2 \end{pmatrix}, \quad \mathbb{T}_{\mathrm{c}} = \rho L_{\mathrm{c}}^2 \begin{pmatrix} \star & 0 & 0 \\ 0 & \star & 0 \\ 0 & 0 & 4\bar{\gamma}_2 \end{pmatrix}, \quad \mathbb{C}_{\mathrm{c}} = \begin{pmatrix} \star & 0 & 0 \\ 0 & \star & 0 \\ 0 & 0 & 4\mu_{\mathrm{c}} \end{pmatrix}. \end{aligned} \tag{4}$$

Only the in-plane components are reported since these are the only ones that play a role in the plane-strain simulations presented in the following sections. The choice of this particular class of symmetry will be justified in the next section by the choice of the unit cell. The action functional $\mathcal{A}$ is thus defined as

$$\mathcal{A} = \iint_{\Omega\times[0,T]} \mathcal{L}\left(\dot{u}, \nabla\dot{u}, \dot{P}, \nabla u, P,\right)\,\mathrm{d}x\,\mathrm{d}t\,, \tag{5}$$

and its first variation $\delta\mathcal{A}$ is taken with respect to the kinematic fields (u, P). Furthermore, it follows from the least-action principle that $\delta\mathcal{A} = 0$ uniquely defines both the equilibrium equations and the boundary conditions (both Neumann and Dirichlet). Thus, the reduced relaxed micromorphic equilibrium equations in strong form are

$$\rho\,\ddot{u} - \mathrm{Div}\widehat{\sigma} = \mathrm{Div}\widetilde{\sigma}\,, \qquad \overline{\sigma} = \widetilde{\sigma} - s\,, \tag{6}$$

where

$$\widetilde{\sigma} := \mathbb{C}_{\mathrm{e}}\,\mathrm{sym}(\nabla u - P) + \mathbb{C}_{\mathrm{c}}\,\mathrm{skew}(\nabla u - P)\,, \quad \widehat{\sigma} := \mathbb{T}_{\mathrm{e}}\,\mathrm{sym}\,\nabla\ddot{u} + \mathbb{T}_{\mathrm{c}}\,\mathrm{skew}\,\nabla\ddot{u}, \tag{7}$$

[2] The higher-order contributions related to Curl P were neglected in the present paper. This choice comes from the observation that, while the curvature term plays a crucial role in the static case (it allows to obtain a specific homogenization formula between the relaxed micromorphic coefficients and the macroscopic stiffnesses when letting $L_{\mathrm{c}} \to 0$), its effect is negligible in the dynamic case. However, it can be inferred (see Table 1 and Eq. (4)) that the introduced inertia terms also introduce a characteristic length L_{c} which is here of the order of the unit cell size.

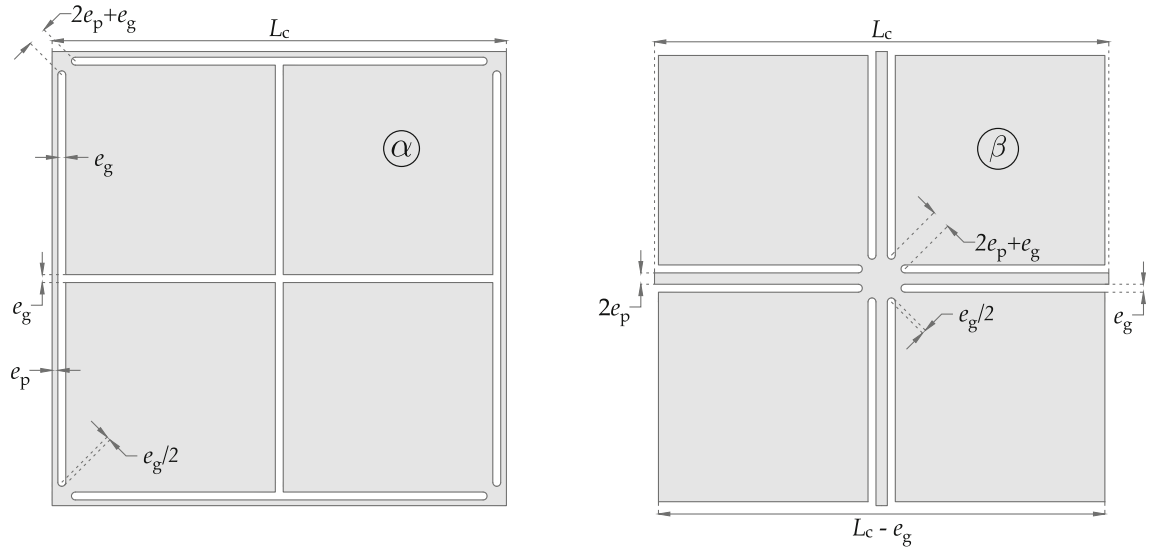

L_c [m]	e_g [mm]	e_p [mm]	ρ_{Ti} [kg/m^3]	κ_{Ti} [Pa]	μ_{Ti} [Pa]
0.02	0.35	0.25	4400	116.7×10^9	41.8×10^9

Fig. 2 (*top left*) unit cell α, (*top right*) unit cell β. The two unit cells are equivalent in the sense that they give rise to the same infinite microstructured material, while giving rise to two finite-size samples with different geometry on the boundary; (*bottom*) material and geometrical properties: the size of the unit cell is L_c, the density ρ_{Ti}, the bulk modulus κ_{Ti} and the shear modulus μ_{Ti}

$$s := \mathbb{C}_{\text{micro}}\,\text{sym}\,P\,, \qquad \overline{\sigma} := \mathbb{J}_m\,\text{sym}\,\ddot{P} + \mathbb{J}_c\,\text{skew}\,\ddot{P}\,. \tag{8}$$

The associated homogeneous Neumann boundary conditions are

$$\widetilde{t} := (\widetilde{\sigma} + \widehat{\sigma})\; n = 0\,, \tag{9}$$

where $\widetilde{t}$ are the generalized traction and n is the normal to the boundary. We also briefly recall here the expression of the traction for a classical *isotropic Cauchy model*

$$t := \sigma\, n\,, \quad \sigma := \kappa\,\text{tr}\,(\nabla u)\;\mathbb{1} + 2\mu\,\text{dev}\,\text{sym}\nabla u\,, \tag{10}$$

where κ and μ are the classical bulk and shear moduli, respectively.

2.1 Identification of the enriched model parameters via dispersion curves fitting

In this section, we briefly present the reduced relaxed micromorphic parameters identification procedure that is done by the means of fitting the dispersion curves. On one hand, the dispersion curves (Fig. 3) of the microstructured material are obtained with a classical Bloch–Floquet analysis performed on any unit cell of the two in Fig. 2 by using *Comsol Multiphysics*®.[3] The two unit cells, which we will name α (*left*) and β (*right*), give rise to the same dispersion curves since a Bloch–Floquet analysis employs periodic boundary conditions, thus mimicking an infinite domain and the two unit cells shown in Fig. 2 are equivalent in the sense that they give rise to the same infinite microstructured material. On the other hand, dispersion curves for the reduced relaxed micromorphic model are obtained analytically by finding the non-trivial solution of the homogeneous equilibrium Eq. (6) under a plane-wave ansatz (for more details, see [86]). The number

[3] The choice of this unit cell is related to the fact that it is the most recent one for which a successful fitting of the RRMM was achieved. Indeed, the RRMM has proven to be successful to describe the response of different tetragonal unit cells and it is not limited to this special case. However, since it is always necessary a preliminary work to perform the reduced relaxed micromorphic model fitting and since we are here interested to study the effect of different cuts in view of gathering better understanding on the effect of boundary conditions on the overall metamaterial's response, we opt for the use of this specific unit cell.

Table 1 Values of the elastic parameters, the micro-inertia parameters, the characteristic length L_c, and the apparent density ρ for the reduced relaxed micromorphic model calibrated on the metamaterial whose building block is any of the two unit cells in Fig. 2

L_c [m]	κ_e [Pa]	μ_e [Pa]	μ_e^* [Pa]
0.02	2.51×10^9	2.39×10^9	1.20×10^6
μ_c [Pa]	κ_m [Pa]	μ_m [Pa]	μ_m^* [Pa]
1.11×10^4	4.54×10^9	4.43×10^9	4.18×10^{10}
κ_γ [–]	γ_1 [–]	γ_1^*[–]	γ_2 [–]
1016.56	983.36	9234.89	0.02
$\overline{\kappa}_\gamma$ [–]	$\overline{\gamma}_1$ [–]	$\overline{\gamma}_1^*$ [–]	$\overline{\gamma}_2$ [–]
5.45	3.09	1.45×10^{-9}	1.87
κ_{Macro} [Pa]	μ_{Macro} [Pa]	μ_{Macro}^* [Pa]	ρ [kg/m^3]
1.62×10^9	1.55×10^9	1.20×10^6	3840.77

In the last row it is reported the *macro-parameters*, i.e., the corresponding long-wavelength limit Cauchy material coefficients [59,67]

of independent parameters in the reduced relaxed micromorphic model is 16: 8 of them can be analytically evaluated or analytically related to the other parameters, while the remaining eight are obtained with an error minimization procedure, so that the dispersion curves issued via the reduced relaxed micromorphic model are the closest possible to those issued via Bloch–Floquet analysis (see Fig. 3). The parameters with an analytical expression are[4]

$$\begin{aligned}
\rho &= \rho_{Ti}\,\frac{A_{Ti}}{A_{tot}}\,, & \kappa_e &= \frac{\kappa_m\,\kappa_{Macro}}{\kappa_m-\kappa_{Macro}}\,, & \mu_e &= \frac{\mu_m\,\mu_{Macro}}{\mu_m-\mu_{Macro}}\,,\\
\mu_e^* &= \frac{\mu_m^*\,\mu_{Macro}^*}{\mu_m^*-\mu_{Macro}^*}\,, & \kappa_\gamma &= \frac{\kappa_e+\kappa_m}{\rho\,L_c^2\,\omega_p^2}\,, & \gamma_1 &= \frac{\mu_e+\mu_m}{\rho\,L_c^2\,\omega_s^2}\,,\\
\gamma_1^* &= \frac{\mu_e^*+\mu_m^*}{\rho\,L_c^2\,\omega_{ss}^2}\,, & \gamma_2 &= \frac{\mu_c}{\rho\,L_c^2\,\omega_r^2}\,.
\end{aligned} \tag{11}$$

where A_{Ti} and A_{tot} are, respectively, the area of titanium and the total area (including the voids) of the unit cell, ω_p, ω_r, ω_s, and ω_{ss} are the cut-off frequencies, namely the frequencies for a vanishing wavenumber $k=0$, κ_{Macro}, μ_{Macro}, and μ_{Macro}^* are the *macro-parameters*, which represent the stiffness of the microstructured material for the long-wavelength limit and can be obtained thanks to the relations of the slope (wave speed) for $k=0$ of the acoustic branches of the dispersion curves (or with classical static test with periodic boundary conditions), while L_c is the length of the side of the unit cell, i.e., $L_c=0.02$ m.

As already remarked, the remaining eight parameters κ_m, μ_m, μ_m^*, μ_c, $\overline{\kappa}_\gamma$, $\overline{\gamma}_1$, $\overline{\gamma}_1^*$, and $\overline{\gamma}_2$ are obtained by minimizing the distance between the dispersion curves obtained via Bloch–Floquet analysis and the ones of the equivalent reduced relaxed micromorphic model through a fitting procedure (for more details see [86]). All the material parameters of the reduced relaxed micromorphic model characterizing the microstructured material of Fig. 2 are summarized in Table 1, and the plots of the two sets of curves are shown in Fig. 3.[5]

[4] As proved in previous papers, when considering the full relaxed micromorphic model in the static case, rigorous homogenization formula relating the micromorphic coefficient to the macro Cauchy limit can be derived when letting the static characteristic length tend to zero (see [22]). We recall here these formulas relating the micromorphic coefficients to the ones associated with the macroscopic Cauchy limit.

[5] The dispersion curves depicted in Fig. 3 represent the first 6 modes of an infinite metamaterial constituted by a periodic repetition of the unit cell in Fig. 3: yellow curves are associated to pressure modes, while red curves represent shear modes. For a direction of propagation of 45°, the acoustic shear and pressure modes are almost superimposed, and the same is for the shear and pressure optic modes starting around 2000 Hz. The band-gap region is highlighted with a light brown color. Clearly, the full microstructured system may exhibit an infinite number of modes when increasing frequency. On the other hand, the considered micromorphic model can only reproduce the first six of these modes. To introduce higher-frequency modes also in the micromorphic modeling framework, extra micro-related degrees of freedom should be introduced with respect to the micro-distortion tensor P alone. However, we are interested in this paper to the lower-frequency behaviors of the considered metamaterial and, in particular, to the possibility of adequately describing dispersion and band gaps in this frequency interval.

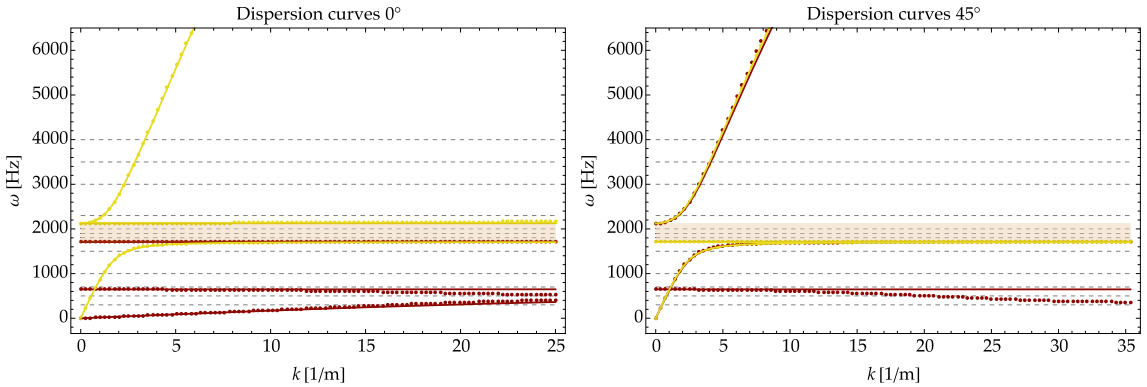

Fig. 3 Dispersion curves for 0°(*left*), and for 45°(*right*). The dots correspond to the solution of the Bloch–Floquet analysis performed on any of the two unit cells in Fig. 2 by using *Comsol Multiphysics*®, while the solid lines represent the analytical expression of the dispersion curves for the reduced relaxed micromorphic model. The dashed lines represent the frequencies used in the numerical simulations

3 Finite element simulations setup

In this section, we present the setting-up of the numerical simulations on a finite-size metamaterial both with a microstructured Cauchy model and the reduced relaxed micromorphic model.

3.1 Microstructured materials simulations setup

All the 2D simulations presented here have been performed under a plane-strain assumption and with a *time-harmonic* ansatz. The two microstructured materials presented in this work have been built as a regular grid of finite-size (16×16 unit cells of side $L_c = 0.02$ m), whose building blocks are the unit cells made up of titanium shown in Fig. 2. The resulting metamaterials are connected to two slender homogeneous Cauchy bars made up of titanium. The following boundary and interface conditions have been enforced (see Fig. 4)

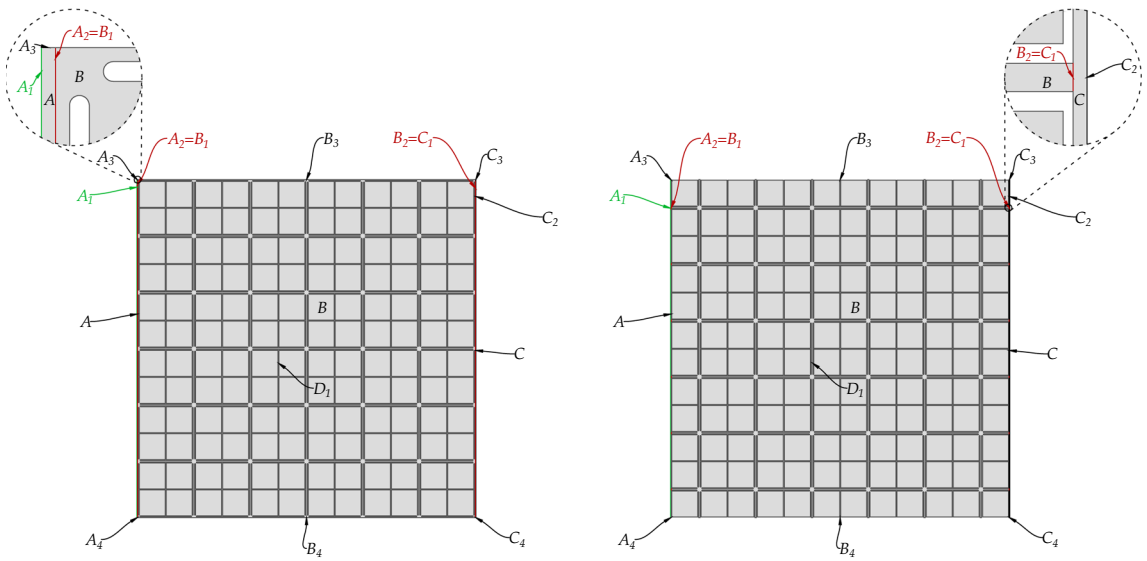

Fig. 4 Schematic view of the geometry and the labeling of the boundaries and interfaces for (*left*) the microstructured material built out of the unit cell α and (*right*) the microstructured material built out of the unit cell β

$$
\begin{array}{rcrcll}
u_1|_{A_1} = \overline{u} & \text{and} & u_2|_{A_1} \rightarrow \text{free} & & \text{(prescribed disp. - green)} & \text{on } A_1 \\
u|_{A_2} = u|_{B_1} & \text{and} & \sigma\, n|_{A_2} = \sigma\, n|_{B_1} & & \text{(perfect contact - red)} & \text{on } A_2 \equiv B_1 \\
u|_{B_2} = u|_{C_1} & \text{and} & \sigma\, n|_{B_2} = \sigma\, n|_{C_1} & & \text{(perfect contact - red)} & \text{on } B_2 \equiv C_1 \\
\sigma\, n = 0 & & & & \text{(stress free - black)} & \text{on } A_3,\, A_4,\, B_3,\, B_4, \\
 & & & & & C_2,\, C_3,\, C_4,\, D_1
\end{array}
\tag{12}
$$

where the magnitude of the harmonic prescribed displacement $\overline{u}$ is 1% of the size of the specimen. In particular we set $\overline{u} = u_0\, e^{-i\omega t}$ with $u0 = 3.2$ mm. The simulations have been performed by using the *Solid Mechanics* physics package of *Comsol Multiphysics*®. In order to ease the convergence of the analysis, we introduced a small amount of numerical isotropic damping ($\eta = 0.002$).

3.2 Reduced relaxed micromorphic continuum simulations setup

The microstructured material is here modeled with the reduced relaxed micromorphic model, which is characterized by the material parameters in Table 1. In addition, the following boundary and interface conditions have been enforced (see Fig. 5)

$$
\begin{array}{rcrcll}
u_1|_{A_1} = \overline{u} & \text{and} & u_2|_{A_1} \rightarrow \text{free} & & \text{(prescribed disp. - green)} & \text{on } A_1 \\
u|_{A_2} = u|_{B_1} & \text{and} & \sigma\, n|_{A_2} = \widetilde{\sigma}\, n|_{B_1} & & \text{(perfect contact - red)} & \text{on } A_2 \equiv B_1 \\
u|_{B_2} = u|_{C_1} & \text{and} & \widetilde{\sigma}\, n|_{B_2} = \sigma\, n|_{C_1} & & \text{(perfect contact - red)} & \text{on } B_2 \equiv C_1 \\
\sigma\, n = 0 & & & & \text{(stress free - black)} & \text{on } A_3,\, A_4,\, C_2,\, C_3,\, C_4 \\
(\widetilde{\sigma} + \widehat{\sigma})\, n = 0 & & & & \text{(stress free - black)} & \text{on } B_3,\, B_4
\end{array}
\tag{13}
$$

where again, the magnitude of the prescribed harmonic displacement $\overline{u}$ is 1% of the size of the specimen. The effective homogeneous material modeled with the reduced relaxed micromorphic model is also embedded between two slender homogeneous Cauchy bars made up of titanium. The simulations have been performed

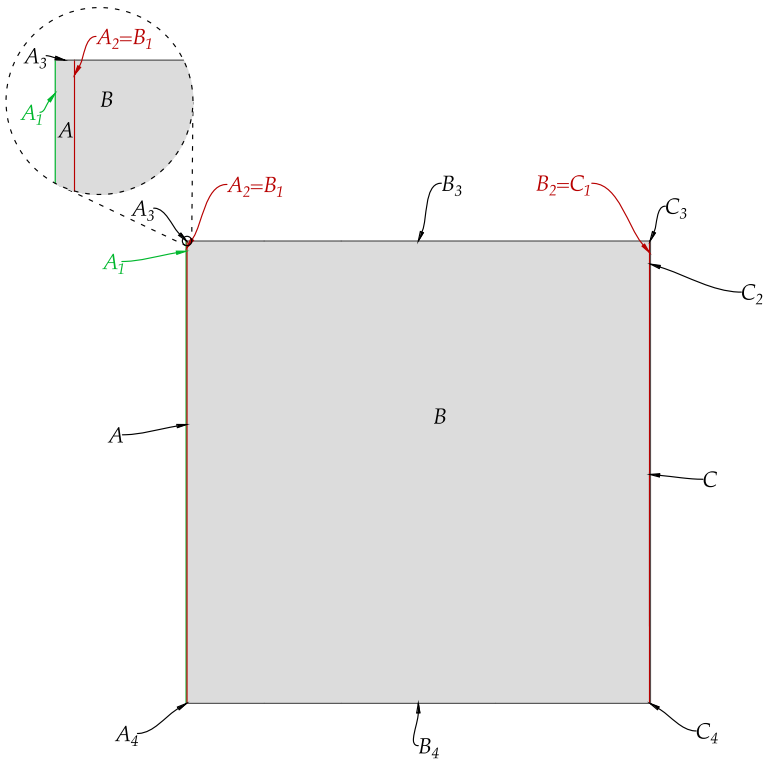

Fig. 5 Schematic view of the geometry and the labeling of the boundaries and interfaces for the equivalent reduced relaxed micromorphic material

by using the *Weak Form PDE* physics package of *Comsol Multiphysics*®. This package requires the implementation of the expression of the Lagrangian (1) and the appropriate boundary and interface conditions. To have a consistent comparison with the results from the microstructured material, we have introduced the same small amount of numerical isotropic viscous damping ($\eta = 0.002$) also in this case.

4 Results and comparison

In this section, we show the results issued by the numerical simulations described in Sect. 3 for the values of frequencies highlighted in Fig. 3 (dashed lines).

In Figs. 6, 7, 8, 9, the structural response for different frequencies is given for (*left*) the microstructured material built out of the unit cell α, (*center*) the equivalent reduced relaxed micromorphic material, and (*right*) the microstructured material built out of the unit cell β. It can be inferred by direct inspection of these figures that the unit cell's cut shown in the *right panel* of Fig. 2 gives rise to a macroscopic response which is better captured by the reduced relaxed micromorphic model, except for the frequency $\omega = 3500$ Hz at which a resonant mode is predominant (see the *right panel* of the second row Fig. 9). However, we can also notice that, except for some small regions close to the boundary, also the behavior of the cut shown in the *left panel*

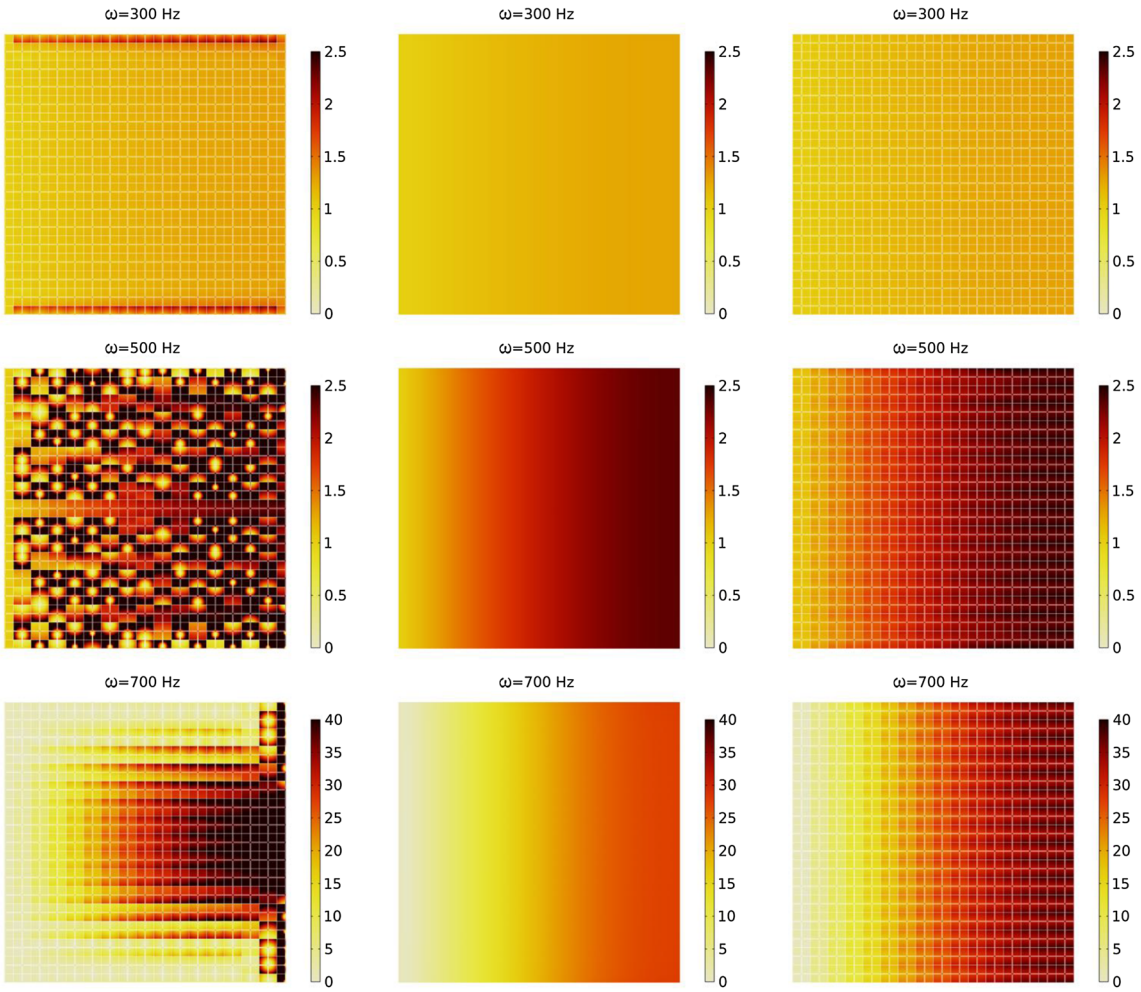

Fig. 6 Norm of the displacement field $|u|$ divided by the amplitude of the assigned harmonic displacement $\overline{u}$ for 300, 500, and 700 Hz for (*left*) the microstructured material whose building block is the unit cell α, (*center*) the equivalent reduced relaxed micromorphic material, and (*right*) the microstructured material whose building block is the unit cell β

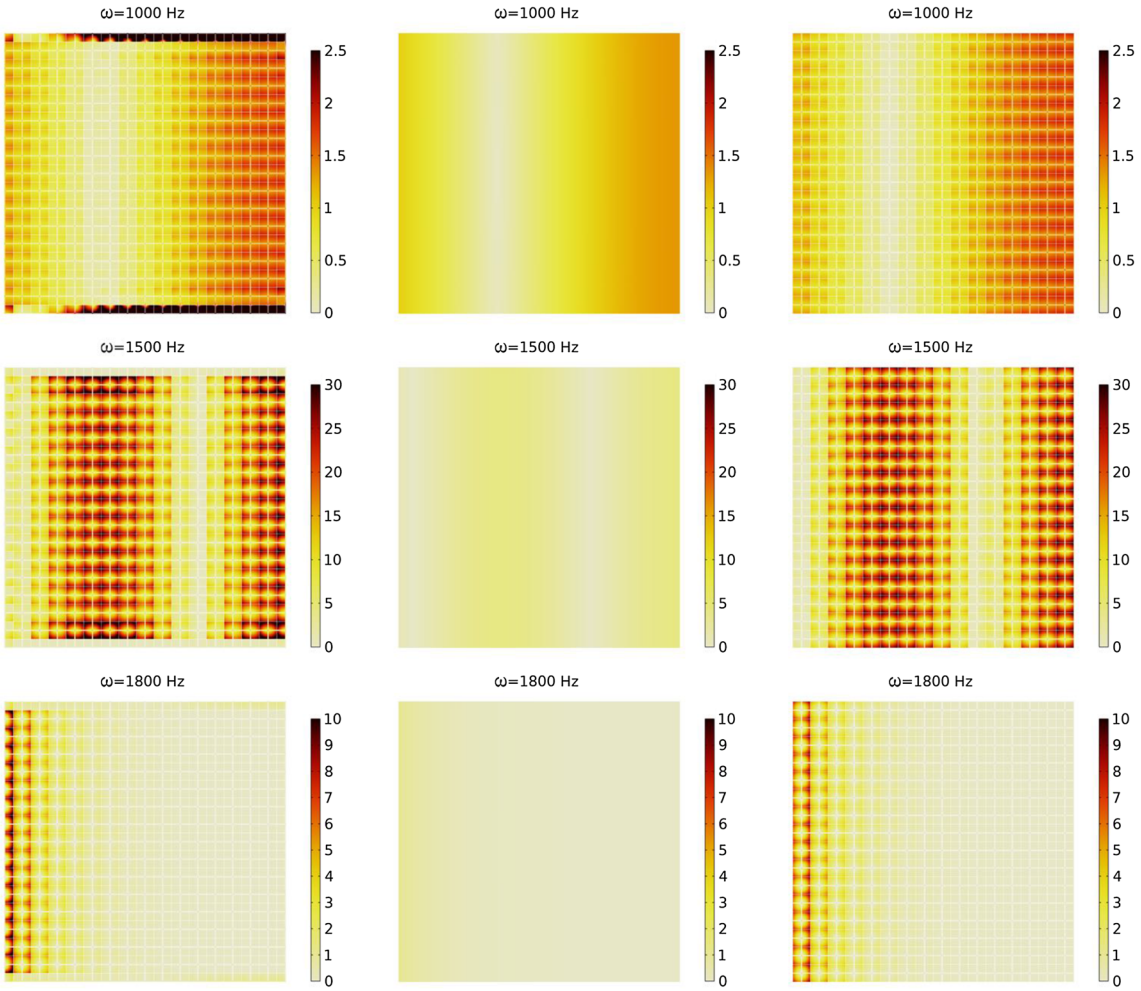

Fig. 7 Norm of the displacement field $|u|$ divided by the amplitude of the assigned harmonic displacement $\overline{u}$ for 1000, 1500, and 1800 Hz for (*left*) the microstructured material whose building block is the unit cell α, (*center*) the equivalent reduced relaxed micromorphic material, and (*right*) the microstructured material whose building block is the unit cell β

of Fig. 2 is captured at an acceptable level of agreement. Exceptions arise for the frequency $\omega = 500$ Hz and $\omega = 700$ Hz at which, once again, microstructure-related resonant modes might become predominant.[6]

[6] Microstructure-related resonant modes are observed by direct inspection of the displacement field inside the unit cell for the microstructured simulation.

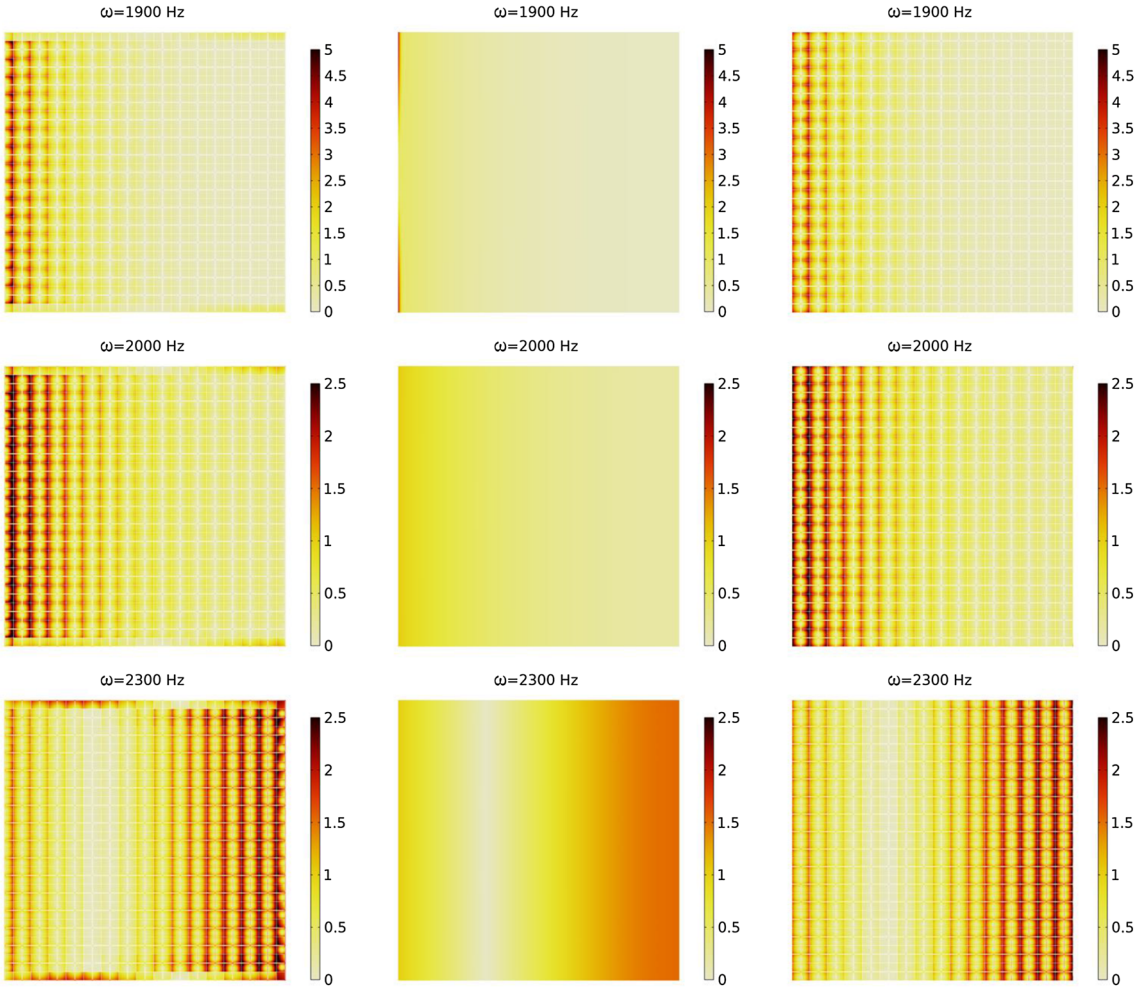

Fig. 8 Norm of the displacement field $|u|$ divided by the amplitude of the assigned harmonic displacement $\overline{u}$ for 1900, 2000, and 2300 Hz for (*left*) the microstructured material whose building block is the unit cell α, (*center*) the equivalent reduced relaxed micromorphic material, and (*right*) the microstructured material whose building block is the unit cell β

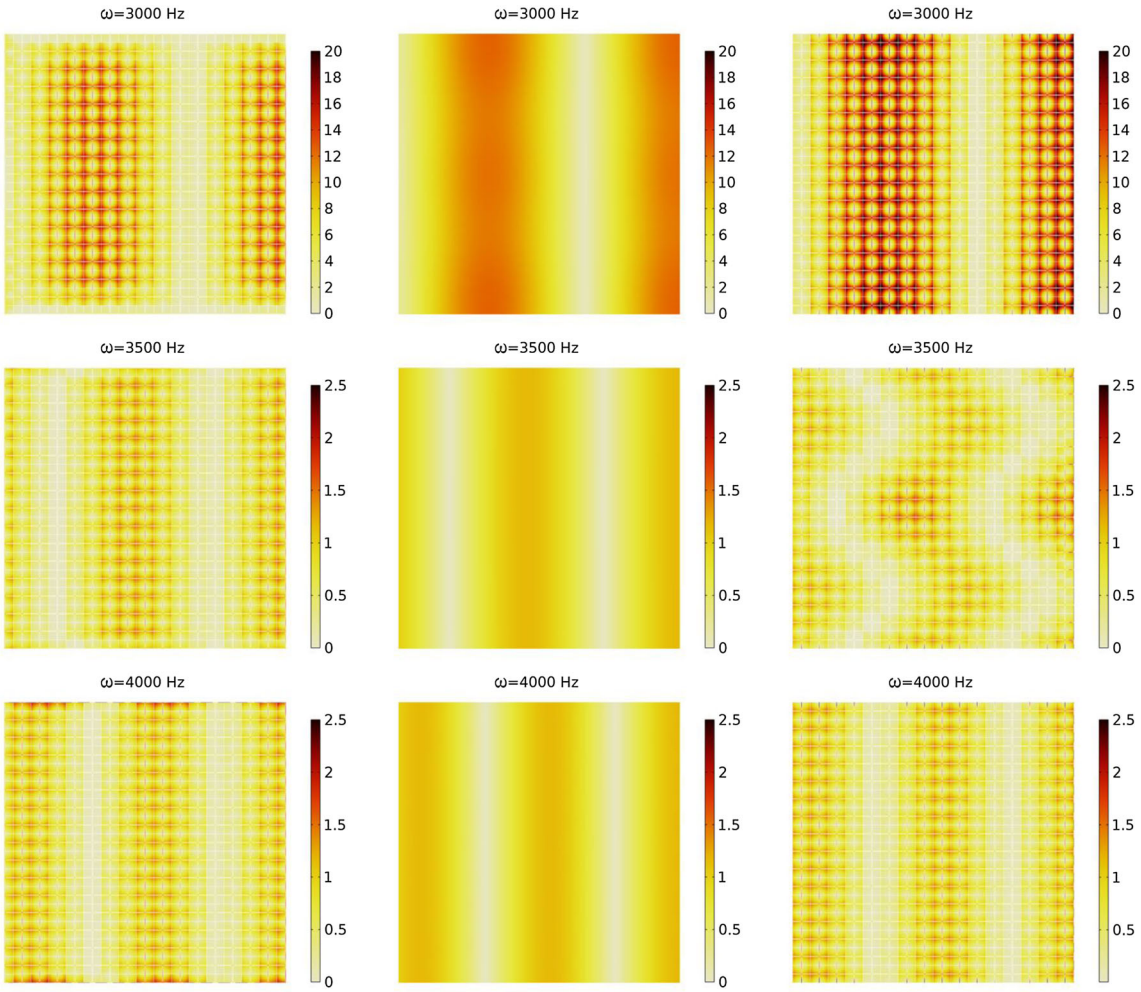

Fig. 9 Norm of the displacement field $|u|$ divided by the amplitude of the assigned harmonic displacement $\overline{u}$ for 3000, 3500, and 4000 Hz for (*left*) the microstructured material whose building block is the unit cell α, (*center*) the equivalent reduced relaxed micromorphic material, and (*right*) the microstructured material whose building block is the unit cell β

5 Discussion

In Fig. 10, we show how the comparison between the total energy of (i) the microstructured material built with the unit cell α (yellow dashed), (ii) the microstructured material built with the unit cell β (black dot-dashed), (iii) the reduced relaxed micromorphic continuum (solid red), and (iv) the equivalent macro Cauchy continuum (green dotted) in the frequency range [0,6000] Hz.

In Figs. 11, 12, 13, we show a detail of the deformation close to the boundary for the simulations at which a disagreement with the reduced relaxed micromorphic model was detected in one of the two microstructured simulations. It seems to be the case that in all the simulations where the macroscopic response of the reduced relaxed micromorphic model deviates from the microstructured one, important bending of the structural elements constituting the unit cell occurs (we better describe this bending in the captions of Figs. 11, 12, 13).

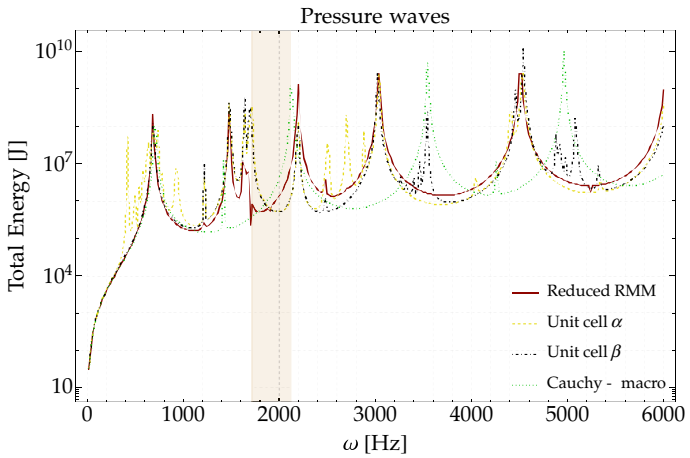

Fig. 10 Comparison between total energy of the microstructured material α (yellow dashed), the microstructured material β (black dot-dashed), the reduced relaxed micromorphic continuum (solid red), and the equivalent macro Cauchy continuum (green dotted) in the frequency range [0,6000] Hz

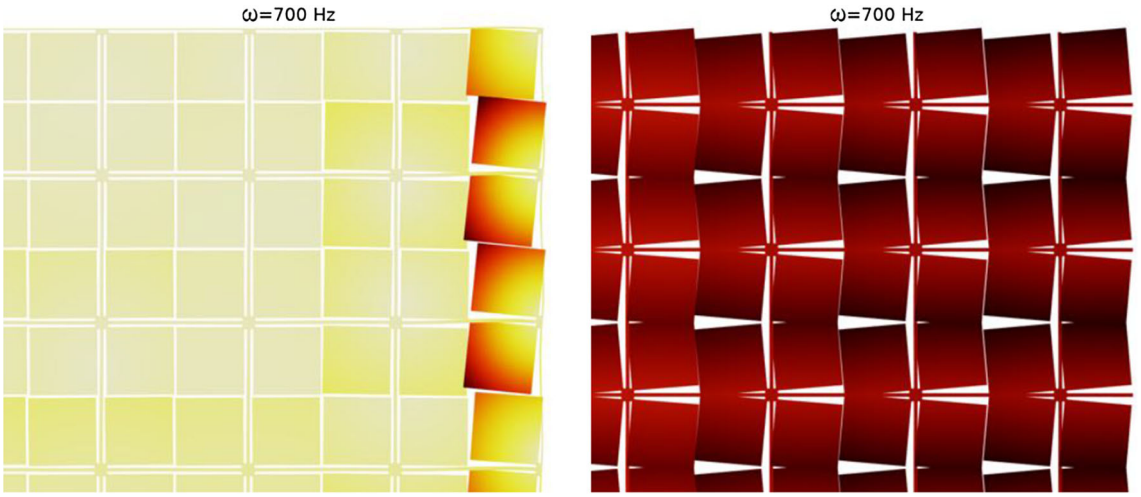

Fig. 11 Detail of the deformation for $\omega = 700$ Hz for (*left*) the structure based on the unit cell α and for (*right*) the structure based on the unit cell β. It can be seen that the unit cell α has a non-symmetric response that propagates along the vertical boundary, while the unit cell β gives clearly rise to a symmetric response. More particularly, in the "symmetric response" (*right*) the internal resonators rotate of the same quantity at the top and at the bottom, so that the thin beams remain undeformed. In the "asymmetric response" (*left*), the rotations of top and bottom element do not compensate each other. This results in the bending of the thin beams inside the unit cell. To make the plot clearer, the homogeneous Cauchy bar at the end of the specimen has been removed from the plot

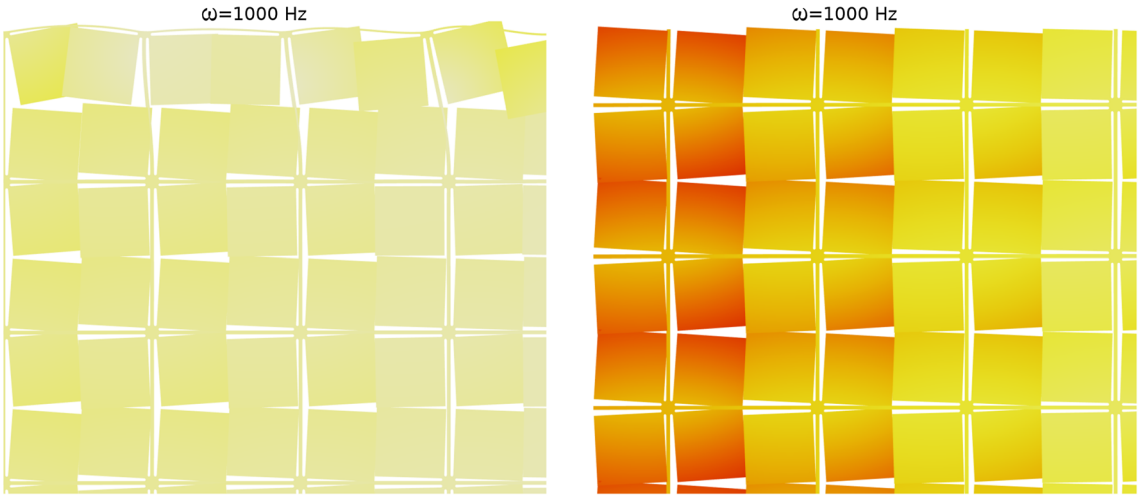

Fig. 12 Detail of the deformation for $\omega = 1000$ Hz for (*left*) the structure based on the unit cell α and for (*right*) the structure based on the unit cell β. It can be seen that the unit cell α has a localized non-symmetric response on the top left corner, while the unit cell β gives clearly rise to a symmetric response. Also in this case, the "non symmetric" response of the resonators implies bending of the thin beams inside the unit cell, while the "symmetric response" leaves the thin beams undeformed. However, the unit cell α recovers a symmetric response while moving away from the boundary. To make the plot clearer, the homogeneous Cauchy bar at the end of the specimen has been removed from the plot

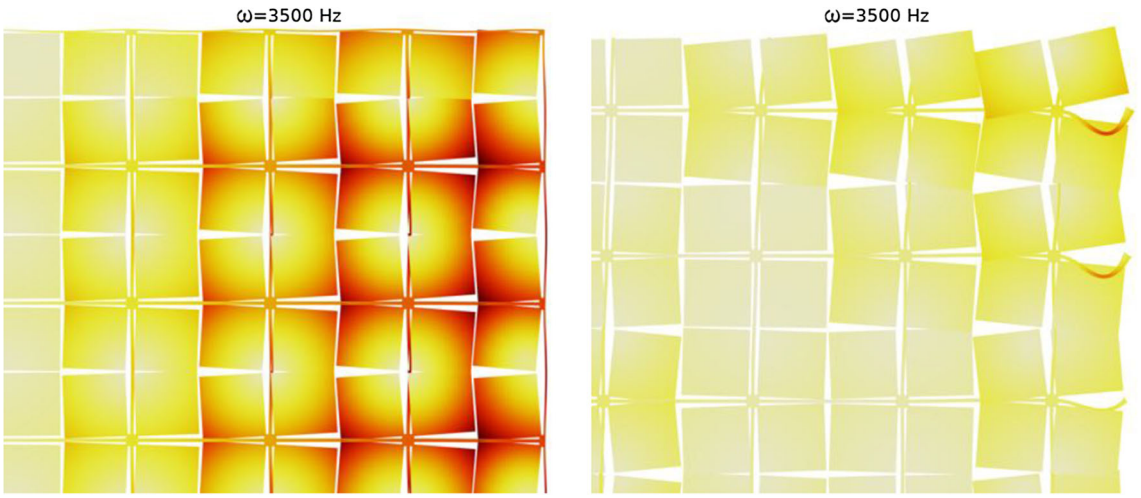

Fig. 13 Detail of the deformation for $\omega = 3500$ Hz for (*left*) the structure based on the unit cell α and for (*right*) the structure based on the unit cell β. It can be seen that the unit cell α has an overall symmetric response on the boundary, while the unit cell β gives clearly rise to a prominent non-symmetric one. Once again the "non symmetric" response gives rise to pronounced bending of the internal thin beams, while the "symmetric response" leaves them almost undeformed. To make the plot clearer, the homogeneous Cauchy bar at the end of the specimen has been removed from the plot

5.1 Effects of the size of the metastructure on the propagation of the boundary localization

In order to further investigate how these boundary effects persist while increasing the size of the domain, we present here the results for an increasingly big metastructure domain for the frequencies $\omega = 500$ Hz and $\omega = 700$ Hz. In Figs. 14, 15 we show how the displacement field changes for a 50×50, a 75×75, and a 100×100 unit cells metastructures: in the top row we report the results for the cut α while in the bottom row the one for the cut β. For $\omega = 500$ Hz, we can see how the boundary effects start to become negligible from a 100×100 unit cells metastructure, while before their effect in the bulk is still relevant. On the contrary, for $\omega = 700$ Hz we can see how the boundary effects start to become negligible from a 75×75 unit cells metastructure, while in a 100×100 their effect is completely relegated to the boundaries and does not affect the bulk material.

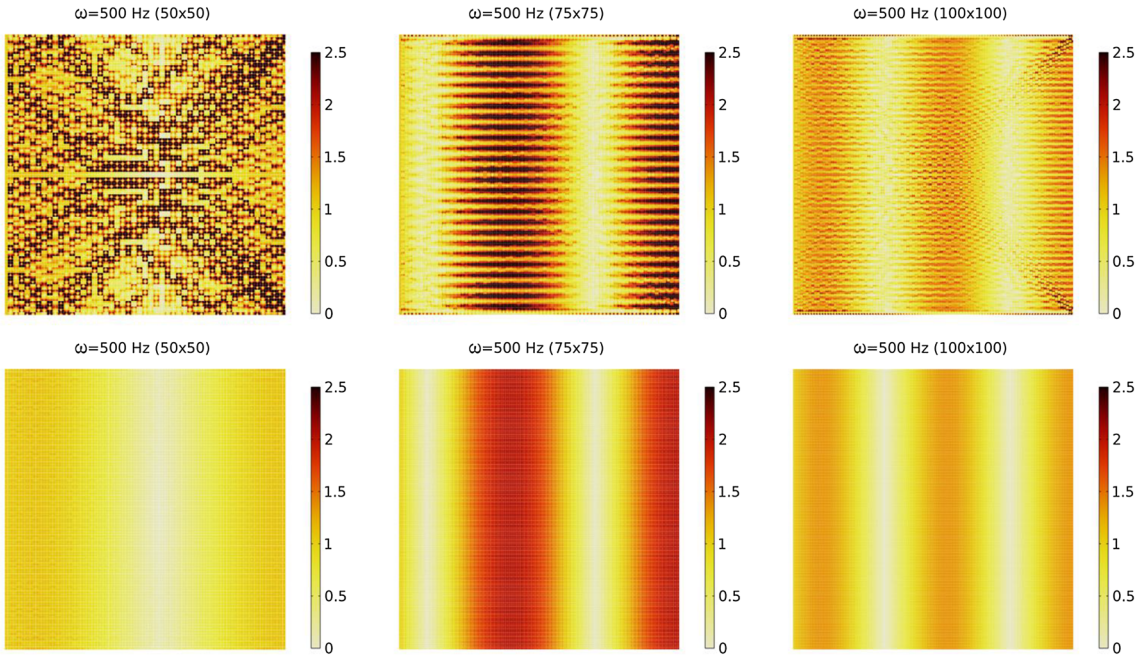

Fig. 14 Norm of the displacement field $|u|$ divided by the amplitude of the assigned harmonic displacement $\overline{u}$ for 500 Hz for (*top*) the microstructured material whose building block is the unit cell α, (*bottom*) the microstructured material whose building block is the unit cell β, for a 50×50, 75×75, and 100×100 unit cells metastructures. The cut α shows an important boundary effect that propagates in the bulk material up to a 100×100 unit cells metastructure, while the cut β does not show noticeable boundary effects regardless the size

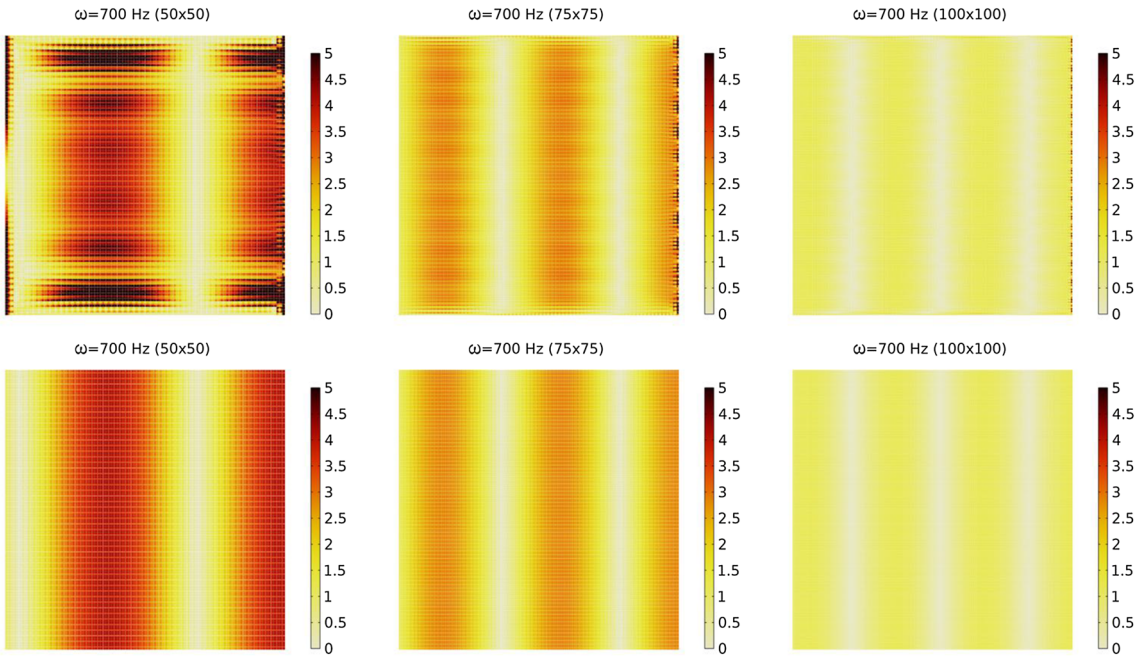

Fig. 15 Norm of the displacement field $|u|$ divided by the amplitude of the assigned harmonic displacement $\overline{u}$ for 700 Hz for (*top*) the microstructured material whose building block is the unit cell α, (*bottom*) the microstructured material whose building block is the unit cell β, for a 50×50, 75×75, and 100×100 unit cells metastructures. The cut α shows an important boundary effect that propagates in the bulk material up to a 50×50 unit cells metastructure while it fades form 75×75. The cut β does not show noticeable boundary effects regardless the size

6 Conclusions

The reduced relaxed micromorphic model has proven to be an effective tool for analyzing and predicting the behavior of microstructured materials also at finite scales. This finding suggests that the enriched model is capable of accurately representing the complex physical interactions and dynamics that occur within these materials, across a broad range of frequencies unless intense small-scale-related resonances are activated. Such a capability is invaluable for developing new technologies and improving existing ones at the scale of the engineers, where a thorough understanding of the behavior of microstructured materials is essential. We showed that when considering simple load conditions and leaving the metamaterial's boundary "free," the reduced relaxed micromorphic model is effective notwithstanding the choice of unit cell "cut." However, the question of how to model the effect of the cell's "cut" in more complex situations (e.g., metamaterial in contact with another solid), remains open. One possible solution could be to enrich the boundary conditions of the reduced relaxed micromorphic model or to explore additional terms introducing specific characteristic lengths. Addressing this issue is critical for achieving even greater accuracy and reliability in modeling microstructured materials and will be addressed in forthcoming papers.

Acknowledgements Angela Madeo, Plastiras Demetriou, and Gianluca Rizzi acknowledge support from the European Commission through the funding of the ERC Consolidator Grant META-LEGO, N° 101001759. The authors also gratefully acknowledge the computing time provided on the Linux HPC cluster at Technical University Dortmund (LiDO3), partially funded in the course of the Large-Scale Equipment Initiative by the German Research Foundation (DFG) as project 271512359.

Funding Open Access funding enabled and organized by Projekt DEAL.

Declarations

Conflict of interest The authors declared that they have no conflicts of interest to this work.

References

1. Aivaliotis, A., Tallarico, D., d'Agostino, M.-V., Daouadji, A., Neff, P., Madeo, A.: Frequency-and angle-dependent scattering of a finite-sized meta-structure via the relaxed micromorphic model. Arch. Appl. Mech. **90**, 1073–1096 (2020)
2. Alavi, S.E., Ganghoffer, J.-F., Sadighi, M.: Chiral Cosserat homogenized constitutive models of architected media based on micromorphic homogenization. Math. Mech. Solids **27**(10), 2287–2313 (2022)
3. Alavi, S., Ganghoffer, J., Reda, H., Sadighi, M.: Construction of micromorphic continua by homogenization based on variational principles. J. Mech. Phys. Solids **153**, 104278 (2021)
4. Alavi, S., Ganghoffer, J., Sadighi, M., Nasimsobhan, M., Akbarzadeh, A.: Continualization method of lattice materials and analysis of size effects revisited based on Cosserat models. Int. J. Solids Struct. **254**, 111894 (2022)
5. Alberdi, R., Robbins, J., Walsh, T., Dingreville, R.: Exploring wave propagation in heterogeneous metastructures using the relaxed micromorphic model. J. Mech. Phys. Solids **155**, 104540 (2021)
6. Allaire, G.: Homogenization and two-scale convergence. SIAM J. Math. Anal. **23**(6), 1482–1518 (1992)
7. Andrianov, I., Bolshakov, V., Danishevs'kyy, V., Weichert, D.: Higher order asymptotic homogenization and wave propagation in periodic composite materials. Proc. R. Soc. A Math. Phys. Eng. Sci. **464**(2093), 1181–1201 (2008)
8. Bacigalupo, A., Gambarotta, L.: Second-gradient homogenized model for wave propagation in heterogeneous periodic media. Int. J. Solids Struct. **51**(5), 1052–1065 (2014)
9. Bensoussan, A., Lions, J., Papanicolaou, G.: Asymptotic Analysis for Periodic Structures. Vol. 374. American Mathematical Soc., (2011)
10. Bilal, O.R., Ballagi, D., Daraio, C.: Architected lattices for simultaneous broadband attenuation of airborne sound and mechanical vibrations in all directions. Phys. Rev. Appl. **10**(5), 054060 (2018)
11. Bordiga, G., Cabras, L., Piccolroaz, A., Bigoni, D.: Prestress tuning of negative refraction and wave channeling from flexural sources. Appl. Phys. Lett. **114**(4), 041901 (2019)
12. Bouchitté, G., Bellieud, M.: Homogenization of a soft elastic material reinforced by fibers. Asymptot. Anal. **32**(2), 153–183 (2002)
13. Boutin, C., Rallu, A., Hans, S.: Large scale modulation of high frequency waves in periodic elastic composites. J. Mech. Phys. Solids **70**, 362–381 (2014)
14. Bückmann, T., Kadic, M., Schittny, R., Wegener, M.: Mechanical cloak design by direct lattice transformation. Proc. Natl. Acad. Sci. **112**(16), 4930–4934 (2015)

15. Camar-Eddine, M., Seppecher, P.: Determination of the closure of the set of elasticity functionals. Arch. Ration. Mech. Anal. **170**(3), 211–245 (2003)
16. Carta, G., Jones, I., Movchan, N., Movchan, A.: Wave polarization and dynamic degeneracy in a chiral elastic lattice. Proc. R. Soc. A **475**(2232), 20190313 (2019)
17. Carta, G., Nieves, M., Jones, I., Movchan, N., Movchan, A.: Flexural vibration systems with gyroscopic spinners. Philos. Trans. R. Soc. A **377**(2156), 20190154 (2019)
18. Celli, P., Yousefzadeh, B., Daraio, C., Gonella, S.: Bandgap widening by disorder in rainbow metamaterials. Appl. Phys. Lett. **114**(9), 091903 (2019)
19. Chen, W., Fish, J.: A dispersive model for wave propagation in periodic heterogeneous media based on homogenization with multiple spatial and temporal scales. J. Appl. Mech. **68**(2), 153–161 (2001)
20. Craster, R., Kaplunov, J., Pichugin, A.: High-frequency homogenization for periodic media. Proc. R. Soc. A Math. Phys. Eng. Sci. **466**(2120), 2341–2362 (2010)
21. Cummer, S.A., Christensen, J., Alù, A.: Controlling sound with acoustic metamaterials. Nat. Rev. Mater. **1**(3), 1–13 (2016)
22. d'Agostino, M.V., Barbagallo, G., Ghiba, I.-D., Eidel, B., Neff, P., Madeo, A.: Effective description of anisotropic wave dispersion in mechanical band-gap metamaterials via the relaxed micromorphic model. J. Elast. **139**, 299–329 (2020)
23. D'Alessandro, L., Zega, V., Ardito, R., Corigliano, A.: 3D auxetic single material periodic structure with ultra-wide tunable bandgap. Sci. Rep. **8**(1), 2262 (2018)
24. Demore, F., Rizzi, G., Collet, M., Neff, P., Madeo, A.: Unfolding engineering metamaterials design: Relaxed micromorphic modeling of large-scale acoustic meta-structures. J. Mech. Phys. Solids **168**, 104995 (2022)
25. El Sherbiny, M., Placidi, L.: Discrete and continuous aspects of some metamaterial elastic structures with band gaps. Arch. Appl. Mech. **88**(10), 1725–1742 (2018)
26. Frecentese, S., Papathanasiou, T., Movchan, A., Movchan, N.: Dispersion of waves and transmission-reflection in blood vessels with structured stents. Proc. R. Soc. A **475**(2223), 20180816 (2019)
27. Frenzel, T., Kadic, M., Wegener, M.: Three-dimensional mechanical metamaterials with a twist. Science **358**(6366), 1072–1074 (2017)
28. Garau, M., Carta, G., Nieves, M., Jones, I., Movchan, N., Movchan, A.: Interfacial waveforms in chiral lattices with gyroscopic spinners. Proc. R. Soc. A Math. Phys. Eng. Sci. **474**(2215), 20180132 (2018)
29. Geers, M., Kouznetsova, V., Brekelmans, M.: Multi-scale computational homogenization: trends and challenges. J. Comput. Appl. Math. **234**(7), 2175–2182 (2010)
30. Ghavanloo, E., El-Borgi, S., Fazelzadeh, S.A.: Formation of quasi-static stop band in a new one-dimensional metamaterial. Arch. Appl. Mech. **93**(1), 287–299 (2023)
31. Ghiba, I.-D., Neff, P., Madeo, A., Placidi, L., Rosi, G.: The relaxed linear micromorphic continuum: existence, uniqueness and continuous dependence in dynamics. Math. Mech. Solids **20**(10), 1171–1197 (2015)
32. Giorgio, I., Rizzi, N., Turco, E.: Continuum modelling of pantographic sheets for out-of-plane bifurcation and vibrational analysis. Proc. R. Soc. A Math. Phys. Eng. Sci. **473**(2207), 20170636 (2017)
33. Goh, H., Kallivokas, L.: Inverse metamaterial design for controlling band gaps in scalar wave problems. Wave Motion **88**, 85–105 (2019)
34. Guenneau, S., Movchan, A., Pétursson, G., Ramakrishna, S.A.: Acoustic metamaterials for sound focusing and confinement. New J. Phys. **9**(11), 399 (2007)
35. Hashin, Z., Shtrikman, S.: A variational approach to the theory of the elastic behaviour of multiphase materials. J. Mech. Phys. Solids **11**(2), 127–140 (1963)
36. He, J.-H., Huang, H.-H.: Complete vibrational bandgap in thin elastic metamaterial plates with periodically slotembedded local resonators. Arch. Appl. Mech. **88**, 1263–1274 (2018)
37. Hill, R.: Elastic properties of reinforced solids: some theoretical principles. J. Mech. Phys. Solids **11**(5), 357–372 (1963)
38. Hu, R., Oskay, C.: Nonlocal homogenization model for wave dispersion and attenuation in elastic and viscoelastic periodic layered media. J. Appl. Mech. **84**(3) (2017)
39. Kaina, N., Causier, A., Bourlier, Y., Fink, M., Berthelot, T., Lerosey, G.: Slow waves in locally resonant metamaterials line defect waveguides. Sci. Rep. **7**(1), 1–11 (2017)
40. Koutsianitis, P., Tairidis, G., Drosopoulos, G., Stavroulakis, G.: Conventional and star-shaped auxetic materials for the creation of band gaps. Arch. Appl. Mech. **89**(12), 2545–2562 (2019)
41. Krödel, S., Thomé, N., Daraio, C.: Wide band-gap seismic metastructures. Extrem. Mech. Lett. **4**, 111–117 (2015)
42. Krushynska, A.O., Bosia, F., Pugno, N.M.: Labyrinthine acoustic metamaterials with space-coiling channels for low-frequency sound control. Acta Acust. United Acust. **104**(2), 200–210 (2018)
43. Lakes, R.: Foam structures with a negative Poisson's ratio. Science **235**(4792), 1038–1040 (1987)
44. Lakes, R.: Experimental evaluation of micromorphic elastic constants in foams and lattices. Z. angew. Math. Phys. **74**(1), 31 (2023)
45. Liu, L., Sridhar, A., Geers, M., Kouznetsova, V.: Computational homogenization of locally resonant acoustic metamaterial panels towards enriched continuum beam/shell structures. Comput. Methods Appl. Mech. Eng. **387**, 114161 (2021)
46. Liu, Z., Zhang, X., Mao, Y., Zhu, Y., Yang, Z., Chan, C.T., Sheng, P.: Locally resonant sonic materials. Science **289**(5485), 1734–1736 (2000)
47. Lustig, B., Elbaz, G., Muhafra, A., Shmuel, G.: Anomalous energy transport in laminates with exceptional points. J. Mech. Phys. Solids **133**, 103719 (2019)
48. Madeo, A., Neff, P., Ghiba, I.-D., Placidi, L., Rosi, G.: Wave propagation in relaxed micromorphic continua: modeling metamaterials with frequency band-gaps. Contin. Mech. Thermodyn. **27**(4), 551–570 (2015)
49. Miehe, C., Schröder, J., Schotte, J.: Computational homogenization analysis in finite plasticity simulation of texture development in polycrystalline materials. Comput. Methods Appl. Mech. Eng. **171**(3–4), 387–418 (1999)
50. Milton, G.: The Theory of Composites. 2002. Cambridge Monographs on Applied and Computational Mathematics (2002)
51. Miniaci, M., Pal, R., Manna, R., Ruzzene, M.: Valley-based splitting of topologically protected helical waves in elastic plates. Phys. Rev. B **100**(2), 024304 (2019)

52. Misseroni, D., Movchan, A., Bigoni, D.: Omnidirectional flexural invisibility of multiple interacting voids in vibrating elastic plates. Proc. R. Soc. A **475**(2229), 20190283 (2019)
53. Misseroni, D., Colquitt, D.J., Movchan, A.B., Movchan, N.V., Jones, I.S.: Cymatics for the cloaking of flexural vibrations in a structured plate. Sci. Rep. **6**(1), 1–11 (2016)
54. Morini, L., Eyzat, Y., Gei, M.: Negative refraction in quasicrystalline multilayered metamaterials. J. Mech. Phys. Solids **124**, 282–298 (2019)
55. Mousanezhad, D., Babaee, S., Ebrahimi, H., Ghosh, R., Hamouda, A.S., Bertoldi, K., Vaziri, A.: Hierarchical honeycomb auxetic metamaterials. Sci. Rep. **5**(1), 1–8 (2015)
56. Movchan, A., Mishuris, G., Sabina, F.: Wave generation and transmission in multi-scale complex media and structured metamaterials (2022)
57. Movchan, A.B., Mishuris, G., Sabina, F.: Wave generation and transmission in multi-scale complex media and structured metamaterials (part 2) (2022)
58. Movchan, A.B., Movchan, N.V., Jones, I.S.: On waves in multi-scale chiral elastic systems. Math. Mech. Solids **27**(9), 1855–1868 (2022)
59. Neff, P., Eidel, B., d'Agostino, M.V., Madeo, A.: Identification of scale-independent material parameters in the relaxed micromorphic model through model-adapted first order homogenization. J. Elast. **139**(2), 269–298 (2020)
60. Neff, P., Ghiba, I.-D., Lazar, M., Madeo, A.: The relaxed linear micromorphic continuum: well-posedness of the static problem and relations to the gauge theory of dislocations. Q. J. Mech. Appl. Math. **68**(1), 53–84 (2015)
61. Neff, P., Ghiba, I.-D., Madeo, A., Placidi, L., Rosi, G.: A unifying perspective: the relaxed linear micromorphic continuum. Contin. Mech. Thermodyn. **26**(5), 639–681 (2014)
62. Norris, A., Amirkulova, F., Parnell, W.: Active elastodynamic cloaking. Math. Mech. Solids **19**(6), 603–625 (2014)
63. Pideri, C., Seppecher, P.: A second gradient material resulting from the homogenization of an heterogeneous linear elastic medium. Contin. Mech. Thermodyn. **9**(5), 241–257 (1997)
64. Ramirez, L.A.P., Rizzi, G., Madeo, A.: Multi-element metamaterial's design through the relaxed micromorphic model. In: Sixty Shades of Generalized Continua: Dedicated to the 60th Birthday of Prof. Victor A. Eremeyev. Springer, pp. 579–600 (2023)
65. Rizzi, G., Dal Corso, F., Veber, D., Bigoni, D.: Identification of second-gradient elastic materials from planar hexagonal lattices. Part I: analytical derivation of equivalent constitutive tensors. Int. J. Solids Struct. **176**, 1–18 (2019)
66. Rizzi, G., Dal Corso, F., Veber, D., Bigoni, D.: Identification of second-gradient elastic materials from planar hexagonal lattices. Part II: mechanical characteristics and model validation. Int. J. Solids Struct. **176**, 19–35 (2019)
67. Rizzi, G., Collet, M., Demore, F., Eidel, B., Neff, P., Madeo, A.: Exploring metamaterials' structures through the relaxed micromorphic model: switching an acoustic screen into an acoustic absorber. Front. Mater. **7**, 589701 (2021)
68. Rizzi, G., d'Agostino, M.V., Neff, P., Madeo, A.: Boundary and interface conditions in the relaxed micromorphic model: exploring finite-size metastructures for elastic wave control. Math. Mech. Solids **27**(6), 1053–1068 (2022)
69. Rizzi, G., Neff, P., Madeo, A.: Metamaterial shields for inner protection and outer tuning through a relaxed micromorphic approach. Philos. Trans. R. Soc. A **380**(2231), 20210400 (2022)
70. Rizzi, G., Tallarico, D., Neff, P., Madeo, A.: Towards the conception of complex engineering meta-structures: relaxed-micromorphic modelling of low-frequency mechanical diodes/high-frequency screens. Wave Motion **113**, 102920 (2022)
71. Rokoš, O., Ameen, M., Peerlings, R., Geers, M.: Extended micromorphic computational homogenization for mechanical metamaterials exhibiting multiple geometric pattern transformations. Extrem. Mech. Lett. **37**, 100708 (2020)
72. Rokoš, O., Ameen, M.M., Peerlings, R.H., Geers, M.G.: Micromorphic computational homogenization for mechanical metamaterials with patterning fluctuation fields. J. Mech. Phys. Solids **123**, 119–137 (2019)
73. Rossi, M., Veber, D., Gei, M.: Numerical assessment of the performance of elastic cloaks for transient flexural waves. Front. Mater. **7**, 603667 (2020)
74. Sánchez-Palencia, E.: Non-homogeneous media and vibration theory. Lecture Notes in Physics 127 (1980)
75. Schwan, L., Favrie, N., Cottereau, R., Lombard, B.: Extended stress gradient elastodynamics: wave dispersion and micro-macro identification of parameters. Int. J. Solids Struct. **219**, 34–50 (2021)
76. Skatulla, S., Sansour, C., Limbert, G.: Local micromorphic non-affine anisotropy for materials incorporating elastically bonded fibres. J. Mech. Phys. Solids **156**, 104576 (2021)
77. Sridhar, A., Kouznetsova, V., Geers, M.: Frequency domain boundary value problem analyses of acoustic metamaterials described by an emergent generalized continuum. Comput. Mech. **65**(3), 789–805 (2020)
78. Sridhar, A., Kouznetsova, V., Geers, M.: A general multiscale framework for the emergent effective elastodynamics of metamaterials. J. Mech. Phys. Solids **111**, 414–433 (2018)
79. Srivastava, A.: Metamaterial properties of periodic laminates. J. Mech. Phys. Solids **96**, 252–263 (2016)
80. Srivastava, A., Nemat-Nasser, S.: On the limit and applicability of dynamic homogenization. Wave Motion **51**(7), 1045–1054 (2014)
81. Srivastava, A., Willis, J.R.: Evanescent wave boundary layers in metamaterials and sidestepping them through a variational approach. Proc. R. Soc. A Math. Phys. Eng. Sci. **473**(2200), 20160765 (2017)
82. Suquet, P.: Elements of homogenization for inelastic solid mechanics, homogenization techniques for composite media. Lect. Notes Phys. **272**, 193 (1985)
83. Tallarico, D., Trevisan, A., Movchan, N.V., Movchan, A.B.: Edge waves and localization in lattices containing tilted resonators. Front. Mater. **4**, 16 (2017)
84. Touboul, M., Cotterill, P.A., Nigro, D., Parnell, W.J.: Enhanced elastodynamic resonance via co-dipole metaclusters. Appl. Phys. Lett. **121**(10), 101702 (2022)
85. van Bree, S., Rokoš, O., Peerlings, R.H., Doškář, M., Geers, M.G.: A Newton solver for micromorphic computational homogenization enabling multiscale buckling analysis of pattern-transforming metamaterials. Comput. Methods Appl. Mech. Eng. **372**, 113333 (2020)
86. Voss, J., Rizzi, G., Neff, P., Madeo, A.: Modeling a labyrinthine acoustic metamaterial through an inertia-augmented relaxed micromorphic approach. Math. Mech. Solids **0**(0), 10812865221137286 (2023)

87. Wang, P., Casadei, F., Shan, S., Weaver, J.C., Bertoldi, K.: Harnessing buckling to design tunable locally resonant acoustic metamaterials. Phys. Rev. Lett. **113**(1), 014301 (2014)
88. Wang, Y., Wang, T., Liang, J., Wang, Y., Laude, V.: Channeled spectrum in the transmission of phononic crystal waveguides. J. Sound Vib. **437**, 410–421 (2018)
89. Willis, J.: Bounds and self-consistent estimates for the overall properties of anisotropic composites. J. Mech. Phys. Solids **25**(3), 185–202 (1977)
90. Willis, J.: Effective constitutive relations for waves in composites and metamaterials. Proc. R. Soc. A Math. Phys. Eng. Sci. **467**(2131), 1865–1879 (2011)
91. Willis, J.: Exact effective relations for dynamics of a laminated body. Mech. Mater. **41**(4), 385–393 (2009)
92. Willis, J.: The construction of effective relations for waves in a composite. C. R. Méc. **340**(4–5), 181–192 (2012)
93. Willis, J.R.: Negative refraction in a laminate. J. Mech. Phys. Solids **97**, 10–18 (2016)
94. Zheng, Y., Niloy, I., Tobasco, I., Celli, P., Plucinsky, P.: Modeling planar kirigami metamaterials as generalized elastic continua. Proc. R. Soc. A Math. Phys. Eng. Sci. **479**(2272), 20220665 (2023)
95. Zhu, R., Liu, X., Huang, G.: Study of anomalous wave propagation and reflection in semi-infinite elastic metamaterials. Wave Motion **55**, 73–83 (2015)